PHYSICAL REVIEW B VOLUME 39, NUMBER 3 15 JANUARY 1989-II

Formation of an interfacial alloy and epitaxial bcc Cr layers on Au(100)

M. C. Hanf, C. Pirri, J. C. Peruchetti, D. Bolmont, and G. Gewinner
Faculté des Sciences et Techniques, Université de Haute Alsace, 4 rue des Frères Lumière, 68093 Mulhouse Cédex, France

(Received 11 April 1988)

We have used angle-resolved photoemission, low-energy electron diffraction, and work-function measurements to probe the crystallographic and electronic structure of the Cr/Au(100) interface formed at temperatures in the 300–500-K range. The first Cr monolayers (ML) diffuse inward and occupy Au lattice sites, forming a random substitutional $Au_{100-x}Cr_x$ fcc alloy with a Cr concentration increasing gradually up to ~50% with increasing Cr coverage. The alloy formation process is diffusion limited and the total amount of Cr involved in the reaction varies from 2–3 ML at 300 K to 4 ML or more at temperatures above 400 K. This metastable epitaxial interfacial alloy exhibits a high structural quality and a large local magnetic moment ($\sim 4\mu_B$) on Cr. Upon further Cr deposition at temperatures below 400 K a disordered Cr-rich phase is first formed in the 4–6-ML range but at 7–8 ML or higher the interfacial alloy behaves as an excellent template for epitaxial growth of well-ordered bcc Cr films. In particular, in the 10–60-ML range the valence-band photoemission spectra are identical to those measured on a single-crystal Cr (100) surface as far as bulk transitions are concerned. Distinct differences visible in the surface electronic structure can be traced back to Au segregation at the film surface as well as a substantial surface roughness. In the 7–10-ML range, important deviations from bulk Cr electronic structure become apparent and the results show a narrowing of the *d* bands and an evolution towards a two-dimensional band structure.

I. INTRODUCTION

Over the last several years, the formation of ordered metal overlayers on single-crystal surfaces has been attracting considerable attention.[1] The restricted geometry in thin films may lead to significant modifications in their electronic properties as compared to the relevant bulk material. In particular, one would like to know how the bulk and surface states evolve as the film thickness is progressively reduced to a few atomic layers. For instance, previous photoemission work has shown that, by ~5 ML, silver on Cu(100) already exhibits a bulklike valence-band structure.[2] However, for free-electron-like *sp* bands which strongly disperse with $k_\perp$, the component of momentum perpendicular to the surface, quantum size effects associated with a discretization of the energy spectrum for a given $k_\parallel$, the component of momentum parallel to the surface, have been observed in thin silver films on Si(111) for thicknesses as large as 15 ML.[13] Ideally, a good system for such studies would be one where the film grows epitaxially in a layer-by-layer mode, exhibits no strain, and does not interact with the substrate.

We present here photoemission measurements on the Cr/Au(100) system which seems interesting for several reasons, including the exceptionally close lattice match (0.02%) for the Au(100)||Cr(100) and Au[010]||Cr[011] epitaxial relationship, a limited overlap in energy of the adsorbate and substrate valence bands, and the fact that Cr is a transition metal showing antiferromagnetism with a small magnetic moment ($\sim 0.6\mu_B$) in its condensed bcc form and a very large moment ($\sim 5\mu_B$) in its atomic form suggesting that interesting magnetic effects might be observed in ultrathin Cr layers. Yet, though earlier work[4–9] assumed generally that the interface formed at 400 K is quite sharp, we have demonstrated recently that alloying with the substrate must occur in order to explain the experimental results.[10] The data presented in this paper confirm that finding and characterize the interfacial compound as an epitaxial random substitutional $Au_{100-x}Cr_x$ fcc alloy ($x \leq 50$) involving 2–3 ML of Cr for room-temperature (RT) grown interfaces and much more at higher temperatures. The photoemission data are actually consistent with solid solution thermodynamic data of Cr in Au and magnetic measurements on the relevant alloys. In spite of the diffuse nature of the interface, we present here clear-cut evidence for epitaxial growth of bcc Cr on top of the interfacial alloy which even at RT acts as an excellent template. While there are indications of a substantial surface roughness implying deviations from simple layer-by-layer growth, the Cr film thickness still appears to be fairly uniform. We were also able to detect significant changes in the bulk electronic structure of these films when their thickness is reduced to ~4 ML corresponding to a total Cr coverage (including the interfacial alloy) of 7–8 ML. These modifications include a narrowing of the *d* bands and a quenching of the photoemission transitions from rapidly dispersing *d* bands.

The outline of the paper is as follows. Section II contains experimental details. In Sec. III we demonstrate and characterize the formation of an interfacial alloy for coverages in the 0–3 ML range. Section IV is mainly devoted to the study of the epitaxial Cr films formed in the 7–60 ML range.

II. EXPERIMENTAL PROCEDURE

The experimental system used for the present investigation includes an UHV chamber equipped with low-energy electron diffraction (LEED), angle-resolved ultraviolet photoemission spectroscopy (ARUPS), and x-ray photoemission spectroscopy (XPS) techniques. Typical angular and energy resolutions are 3° (15°) and 200 meV (1000 meV) (full width at half maximum), respectively, in ARUPS (XPS). Absolute values for the work function Φ were evaluated by measuring the width of the photoemission energy distribution curves at normal emission with the sample negatively biased (-10.00 V) with respect to the ground.

A Au single crystal cut within 0.5° of the (100) orientation was mechanically polished with 0.5-μm diamond paste and chemically polished prior to insertion into the vacuum system. Under ultrahigh-vacuum conditions the sample was repetitively cleaned with 600-eV Ar ions sputtering and annealing at 800 K until the surface showed the characteristic (5×20) LEED pattern and no impurities could be detected by XPS or UPS. Cr layers in the 0–60 ML range, as monitored by a calibrated quartz balance, were condensed onto the surface held at temperatures between 300 and 500 K from a Cr source operating at a typical rate of 0.5 ML/min [1 ML equivalent to the surface density of Au(100)] and at a pressure of 5×10^{-10} Torr. Most of the data presented here are for a substrate held at RT.

Epitaxial $\text{Au}_{100-x}\text{Cr}_x$ alloys on Au(100) were also prepared by coevaporation of Au and Cr onto Au(100). The thickness was about 20 Å and the concentration x was estimated either from the Au and Cr evaporation rates or by means of core-level intensity measurements. The x values inferred from these methods are in reasonable agreement and the absolute uncertainty is ~5 at. %. Even with the substrate at RT during evaporation, the alloy surface exhibited a good (100) (1×1) LEED diagram indicating that the alloy grows epitaxially on Au(100) provided that $x \le 50$. For $x > 50$, no ordered LEED pattern can be seen suggesting the formation of a disordered phase. This behavior is in agreement with the Au-Cr phase diagram which indicates first that a fcc $\text{Au}_{100-x}\text{Cr}_x$ phase with $x \ge 47$ exists with a lattice parameter close to that of pure Au, and second that no ordered Cr-rich phase can be formed, the solubility of Au in bcc Cr being actually quite small (≤ 0.05 at. %). The $\text{Au}_{100-x}\text{Cr}_x$ ($x \le 50$) alloy formed by coevaporation on Au(100) at temperatures in the 300–400-K range was a random substitutional alloy since no superstructure could be detected by LEED.

Angle-resolved photoemission spectra were also recorded from clean Cr(100). The chromium single crystal was spark cut after orientation and mechanically and electrolytically polished using standard techniques. The *in situ* cleaning procedure has been described in detail elsewhere.[11–13]

III. FORMATION OF AN INTERFACIAL ALLOY

A. Valence-band structure

The alloying of the first monolayers of Cr deposited on clean Au(100) is demonstrated in Fig. 1 which presents a series of spectra taken at normal emission with $\hbar\omega=16.8$ eV photons. The substrate temperature is held at RT but similar results are observed at 400 K. Features at 2.6-, 3.5-, 6.3-, and 7.2-eV binding energies (BE) on clean Au(100) (5×20) are transitions from Au $5d$ bands. Deposition of 1 ML of Cr results in the appearance of a new feature near 0.8 eV and changes in the Au $5d$ emission, in particular, the suppression of the Au $5d$ transitions in the valley between the 2.8- and 3.5-eV peaks. LEED indicates a reversion of the (5×20) to a (1×1) surface structure on Cr deposition in the submonolayer range in agreement with previous studies.[4,14] This structural conversion is accompanied by a change in $k_{\parallel}$ selection rules and surface electronic structure which explain the modification observed at this stage in the Au $5d$ band.[15] The Cr-induced feature at 0.8 eV has essentially the same width and position as observed in previous photoemission work on $\text{Au}_{90}\text{Cr}_{10}$ alloys by Reehal and Andrews.[16] This points towards surface alloying but does not prove it since isolated Cr species on the surface are expected to give a similar virtual bound-state feature in photoemission.[17,18] However, the important point here is that the Cr $3d$ feature becomes broader, shifts to ~1.0 eV BE but persists on increasing the Cr coverage up to ~3 ML. Actually a much larger Cr $3d$ band should be formed above 1 ML if the interface were sharp. Moreover, it is quite apparent in Fig. 1 that the Au $5d$ features do not show the uniform attenuation expected in the case of a simple layer-by-layer overgrowth. Note, for instance, the drastic decrease of the high-lying 2.6-eV feature with increasing Cr coverage in contrast with the lower-lying transitions at 3.5, 6.3, and 7.2 eV. Additionally there is a distinct shift towards higher binding ener-

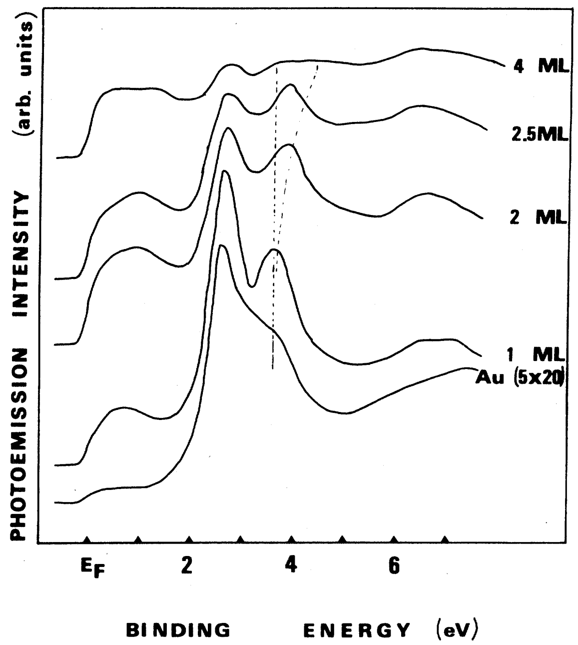

FIG. 1. Normal emission spectra taken with $\hbar\omega=16.8$ eV for various Cr coverages of the Au(100) substrate held at RT.

gies of the feature located at 3.5 eV BE on clean Au(100).

These data strongly suggest the formation of an interfacial alloy. In order to demonstrate this effect unambiguously we compare in Fig. 2 the spectra taken at normal emission with 21.2-eV photons for 1, 2, and 3 ML of Cr deposited on Au(100) held at room temperature, on the one hand, and coevaporated $Au_{100-x}Cr_x$ alloys with $x=15$, 30, and 45, on the other hand. It is obvious that there is a striking similarity. One observes essentially a one-to-one correspondence between the spectra of these series. The difference apparent in the 6.3-eV peak height comes form a contribution of the pure Au(100) substrate in the case of Cr/Au(100) where the interfacial alloy thickness is comparable to the electron escape depth. Figure 2 also shows that in the alloy the Au 5*d* band becomes narrower and moves to higher BE as the Au concentration decreases. The high-lying $5d_{5/2}$ spin-orbit-split part near 3.8 eV is more strongly affected by the alloying process than the low-lying $5d_{3/2}$ features at 6.3 and 7 eV. This behavior along with a general smearing out of the host band structure relative to the pure metal case has been reported before for Au alloys.[19,20] In the dilute limit (small *x* or submonolayer coverages) the Cr 3*d* feature near 0.8 eV is a virtual bound state which can be identified with the occupied part of the spin-split Cr 3*d* states since, as shown below, in such alloys the Cr species carry a large local magnetic moment. With increasing Cr concentration Friedel's virtual bound-state model[21] must be replaced by a split-band model[22,23] which describes concentrated alloys when the atomic number difference is large as in the case of Au and Cr. It is clear from Figs. 1 and 2 that the concept of $Au_{100-x}Cr_x$ valence bands split into two resolvable components at different energies offers an appropriate description of the photoemission spectra. Each component is identified with electrons having greater probability density at the relevant metal site. The Cr 3*d* derived states form a narrow band near 1 eV BE because the interatomic distance is large (~2.88 Å) relative to the bcc Cr bulk lattice spacing (~2.49 Å). The Au 5*d* states, however, still form a rather large band since 5*d* orbitals are less localized and the interatomic distance in these alloys is close to that of pure Au.[24]

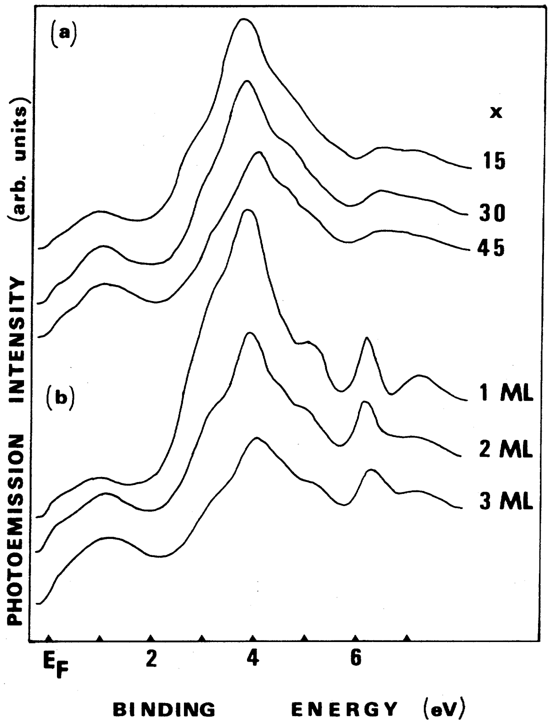

FIG. 2. Normal emission spectra taken with $\hbar\omega=21.2$ eV: (a) 20 Å of coevaporated epitaxial $Au_{100-x}Cr_x$ alloy films on Au(100), (b) Cr deposited on Au(100) kept at RT.

Thus, the data of Figs. 1 and 2 imply the formation of a $Au_{100-x}Cr_x$ alloy at the Cr/Au(100) interface with *x* increasing progressively up to ~50 with increasing Cr coverage. LEED observations show a good (1×1) pattern over the whole coverage or concentration range. We therefore conclude that the interfacial $Au_{100-x}Cr_x$ alloy must be an epitaxial random substitutional alloy with Cr. species occupying sites of the fcc Au lattice, in agreement with the Au-Cr phase diagram which indicates a solubility limit of Cr in fcc Au of 47 at.%. According to Miedema's semiempirical scheme the solution energy for Cr in Au is indeed negative: $E_s(\mathrm{Cr/Au})=-0.01$ eV/atom.[25] Thus, the alloying process observed at the Cr/Au(100) surface is not surprising. In principle, for a given Cr deposit interdiffusion will continue until the substrate becomes a dilute alloy of the two materials. However, near RT the small diffusion coefficient limits the formation of the epitaxial substitutional alloy, which stops once the solubility limit is reached in the overlayer. For the RT-formed interface, this happens when the Cr coverage approaches 3 ML. Indeed, it can be seen in Fig. 1 that by 4 ML the single Cr 3*d* peak near 1 eV characteristic of the alloy is replaced by two structures near 0.6 and 1.3 eV suggesting that the interaction between Cr species now becomes much stronger.

B. Magnetic properties

The $Au_{100-x}Cr_x$ alloys are known to be magnetic. Magnetic and neutron-diffraction measurements reveal a spin-glass behavior at dilute Cr concentrations ($x\le10$) and a nature of long-range antiferromagnetism at high concentrations.[26,27] The magnetic interaction is of the Ruderman-Kittel-Kasuya-Yosida (RKKY) type between localized Cr moments via conduction electrons. Figure 3 shows some typical Cr 2*s* spectra which demonstrate that the Cr atoms, indeed, carry a high local magnetic moment up to several monolayers of Cr on Au(100). To determine the multiplet splitting, the spectra were fitted to two Gaussians as shown in the case of 3 ML deposited on the substrate held at 480 K. A good fit is obtained for a splitting $\Delta E_{2s}=5.1\pm0.2$ eV and relative intensities of the components of ~1.5/1. The multiplet splitting arises from the exchange interaction between the single 2*s* electron left behind after the photoemission process and the magnetic moment of the unfilled 3*d* valence subshell. Van Vleck's formula[28] gives

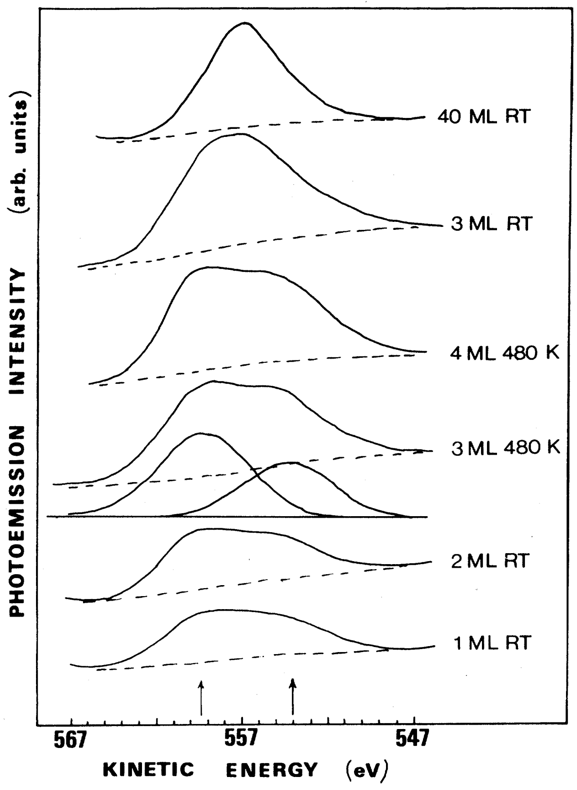

FIG. 3. Cr 2s core line photoemission spectra excited with unmonochromatized Mg $K\alpha$ radiation for various coverages and substrate temperatures. A nonlinear mean-squares fit of two Gaussians was used to determine the multiplet separation as shown for 3 ML deposited on the substrate held at 480 K. Note the Cr 2s core line shape in the case of 3 ML deposited on the substrate at RT, due to the presence of a Cr-rich phase on top of the interfacial alloy.

$$\Delta E_{2s}=\frac{2S+1}{5}G^2(2s,3d) ,$$

where S is the resulting spin of the initial state and $G^2(2s,3d)$ is a Slater exchange integral. This is a good quantitative approximation for interaction between subshells of different principal quantum numbers.[29] Assuming a constant $G^2(2s,3d)$, a simple comparison with the case of Cr_2O_3 where $S=\frac{3}{2}$ (Cr^{3+}) and $\Delta E_s \approx 4.1$ eV (Ref. 30) yields $S\approx 2.0$ for Cr in $Au_{100-x}Cr_x$. Converted into a magnetic moment, this corresponds to $\sim 4\mu_B$ ($4.9\mu_B$ effective moment). This is in reasonable agreement with the value of $4.1\mu_B$ inferred from magnetic measurements by Wachtel and Vetter.[26] Note also the multiplet branching ratio of $(S+1)/S=\frac{3}{2}$ in good agreement with the observed ratio. The data of Fig. 3 indicate that the magnetic moment does not change substantially with x or coverage as long as the Cr species are indeed accommodated in the substitutional alloy. The 480-K spectra, for instance, only reveal a very small decrease (nonsignificant within the present approximations) in multiplet splitting in the 0–4-ML coverage range. This shows that at such temperatures at least 4 ML of Cr are readily incorporated into the Cr lattice. In contrast, for the room-temperature data it is found that by 3 ML a simple fit to two Gaussians is no longer satisfactory. In fact, at this stage the spectrum can be represented by the sum of the two Gaussians describing the multiplet components of Cr in the interfacial alloy and a third component which resembles the Cr 2s spectrum of bulk bcc Cr. This suggests that a new Cr-rich phase definitely different from fcc $Au_{100-x}Cr_x$ ($x \leq 50$) must be present on top of the interfacial alloy since we expect the drastic reduction in multiplet splitting to be connected with enhanced Cr-Cr interactions. Again we find that by 3 ML deposited on the substrate held at RT, the limiting solubility of Cr in Au is already reached in the overlayer.

The magnetic properties of the alloy are reflected in other Cr core lines too. The example of Cr $2p_{3/2}$ is shown in Fig. 4 which presents a series of spectra versus Cr coverage for a substrate held at RT. In the alloying regime it can be seen that the line exhibits a broad asymmetric shape with some resolved structure because of the exchange interaction of the 2p hole with the open 3d shell. As demonstrated previously in the case of MnF_2, a large number of multiplets is distributed over the whole $2p_{3/2}$-$2p_{1/2}$ spectral domain.[31] However, for a quantitative interpretation, detailed calculations of the p^5d^n configuration energy levels must be performed similar to those reported by Gupta and Sen[32] for $n=5$. An interesting consequence of the presence of these multiplets in the Cr2p spectrum is an apparent increase in the spin-orbit splitting as measured between the centroids of the

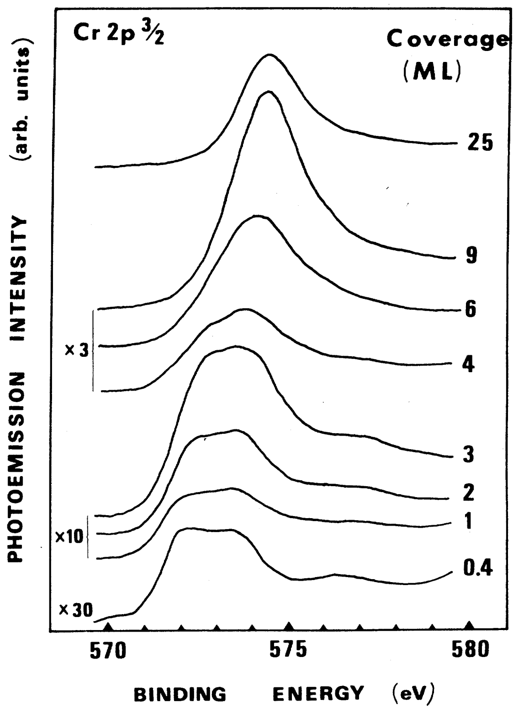

FIG. 4. Cr $2p_{3/2}$ core line photoemission spectra excited with $\hbar\omega=1253.6$ eV for various coverages of Cr on Au(100) held at RT.

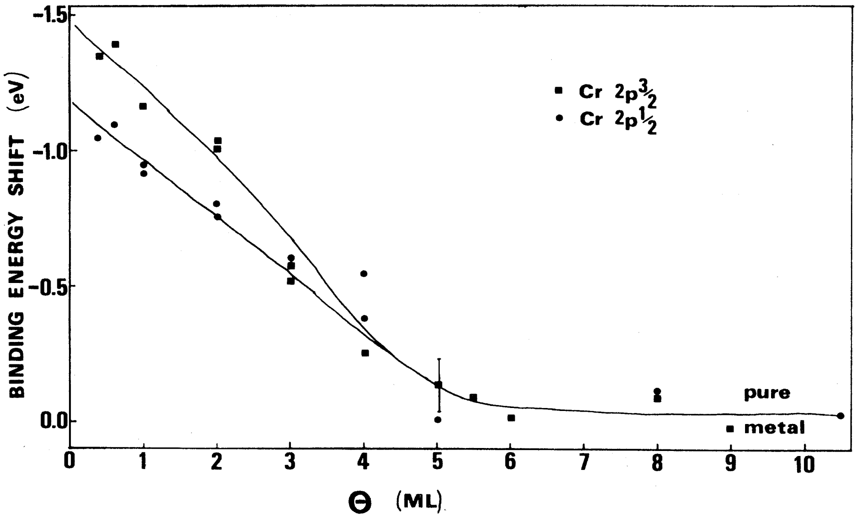

FIG. 5. Binding-energy shifts relative to pure Cr metal for the Cr $2p_{1/2}$ and Cr $2p_{3/2}$ core lines vs Cr coverage of Au(100). These shifts are taken from difference spectra, as explained in the text, in order to reflect the properties of the topmost layer.

$2p_{3/2}$ and $2p_{1/2}$ components.[31] The exchange interaction breaks the degeneracy of J with the states of higher J shifting to lower binding energy for $2p_{3/2}$ and to higher binding energy for $2p_{1/2}$. Note that the apparent increase in spin-orbit splitting is a good measure of the amount of unpaired spin on a Cr site.

C. Core-level shifts

Figure 4 indicates a drastic core-level shift for the first Cr monolayers deposited on Au(100). Again the persistence of an important shift up to several Cr monolayers implies Au-Cr alloying. Figure 5 presents the Cr $2p_{3/2}$ and Cr $2p_{1/2}$ core-level shifts relative to bulk bcc Cr as a function of coverage Θ. These data are obtained as follows. For $\Theta < 1$ ML, the shift is merely determined from peak centroid location in the rough spectrum. For $\Theta > 1$ ML, however, the value indicated for Θ is inferred from peak centroid location of the difference spectrum obtained by subtracting the spectrum for $\Theta - 1$ with the appropriate attenuation from that for Θ. In this way the data in Fig. 5 reflect the core-level shift in the topmost layer rather than a weighted average over the whole overlayer thickness which is much smaller than the depth probed by XPS. The difference between Cr $2p_{3/2}$ and Cr $2p_{1/2}$ data reveals the apparent increase in spin-orbit splitting reflecting the magnitude of the local magnetic moment on the Cr sites.

For B species embedded in an $A_{100-x}B_x$ alloy the core-level shift is a function of x which drops progressively from a maximum value in the dilute case (small x) to zero for pure B.[33] Thus, the data of Fig. 5 suggest that the Cr concentration in the top layer of the interfacial $\mathrm{Au}_{100-x}\mathrm{Cr}_x$ rises progressively with Θ. A concentration gradient normal to the surface is apparently established, as expected for a diffusion-limited alloying process. The observed sign and magnitude of the Cr $2p$ core line shift can be qualitatively predicted from a thermodynamic model. It can be shown that within the equivalent-cores approximation, the core-level shift is closely related to thermodynamical properties by means of Born-Haber cycles. In the case of alloys, the core line shift relative to the pure element is expressed in the heats of formation of binary compounds weighted by environment factors.[33] Let us just consider here the initial shift which corresponds to the dilute alloy case ($x \rightarrow 0$) developed in Ref. 34. In that case the binding-energy shift is

$$\Delta E = +E(\mathrm{Mn},\mathrm{Au}) - E(\mathrm{Mn},\mathrm{Cr}) - E(\mathrm{Cr},\mathrm{Au}) ,$$

where $E(A,B)$ is the solution energy of a metallic atom A in a matrix B. Using the solution energies calculated with the semiempirical scheme of Miedema[25] one gets $\Delta E = -0.50$ eV. This is significantly lower than experiment (-0.90 eV for Cr $2p_{1/2}$) but yields the right sign and order of magnitude. Note that in Miedema's theory of solution energies the alloys are taken in their liquid phase and that thermodynamical entities are thermal excitation energies as opposed to core-level shifts which correspond to vertical excitation energies.[34]

Another approach to the interpretation of core-level shifts is the classical chemical shift point of view in which the potential at the Cr atom embedded in Au is altered by charge transfer to or from the solute. In this picture, since Au has the highest electronegativity one would expect a core-level shift to higher (lower) binding energies for Cr (Au), exactly the opposite to the observed behavior. Actually, this simple relationship is often not observed experimentally[35,36] and the potential felt by a core electron of a given species is determined by the character of the acceptor or donor (s-, p-, or d-like) orbital rather than the total charge transferred.[36] The problems associated with relating chemical shifts in alloys to charge flow was considered in some detail for gold alloys by Watson *et al.*[37] Mössbauer isomer-shift data, which are measurements of electron density at the nucleus, indicate a substantial flow of s-like electron charge (up to one $6s$ electron) onto Au on alloying, as expected from electronega-

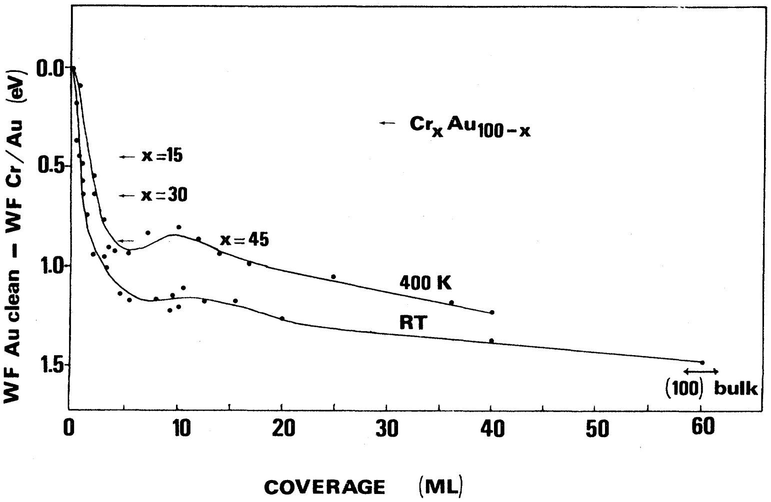

FIG. 6. Change in work function vs Cr coverage of Au(100) held either at RT or 400 K during deposition.

tivity considerations. However, this is accompanied by a compensating depletion of d charge and it turns out that these competitive d effects actually determine the core-level shifts. Note that the Coulomb interaction of the core state is stronger with d-like than s-like valence states. For Au in $Au_{100-x}Cr_x$ the measured shift relative to pure Au is $\Delta E(4f)=+0.50$ eV for $x\approx 45$. According to the above considerations, the total charge transfer is relatively small and a substantial atomic configuration change relative to the pure metal case must occur for both partners upon alloying. In the present case, the charge transfer is $s\rightarrow d$ for Cr and $d\rightarrow s$ for Au species. This result suggests that the $d^{5-\epsilon}s^{1+\epsilon}$ configuration of Cr metal evolves towards the free-atom configuration upon alloying with Au. In this regard, note the large local magnetic moment carried by the Cr species, close to the value of the free-atom $d^5(^6S)$ ground state.

D. Work-function measurements

Figure 6 presents the work function versus coverage for two substrate temperatures: RT and 400 K. In the alloying there is a sharp reduction in work function with increasing coverage. The relevant data for coevaporated $Au_{100-x}Cr_x$ are also shown for $x=15$, 30, and 45. It can be seen that these data essentially confirm the relationship between Cr coverage on Au(100) and Cr concentration in the superficial $Au_{100-x}Cr_x$ alloy as found in Secs. III A and III B. We again come to the conclusion that at RT the limiting solubility must be reached in the 2–3-ML range. Clearly the temperature strongly affects the work-function data. It is apparent that the work function and in turn the Au concentration in the overlayer is higher at 400 K than at RT. One reason for that behavior is obviously the enhanced diffusion at 400 K which results in a lower mean Cr concentration in the alloy overlayer. The second reason is that there is a strong tendency for Au segregation at the $Au_{100-x}Cr_x$ surface, forming Au (100) patches particularly at 400 K and above. This is demonstrated in detail elsewhere[10,14] in relation with the remarkable persistence of the Au(100) (1×1) $\bar{M}_3$ surface state at the Cr/Au(100) interface first observed by O'Neill and Weaver.[38] Clearly, considering the high surface energy of Cr (a midseries transition metal), the segregation

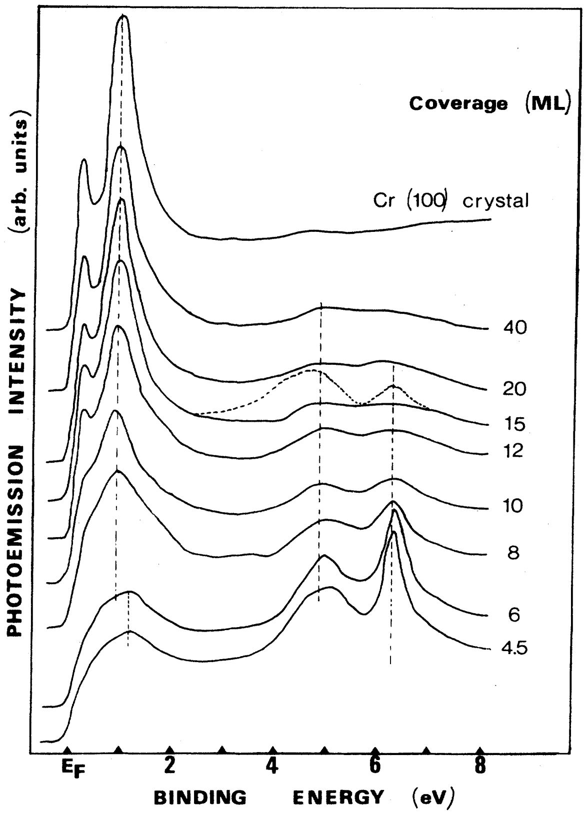

FIG. 7. Off-normal emission spectra taken with $\hbar\omega=21.2$ eV for various Cr coverages of Au(100). The emission plane is (001) and the polar angle of emission is 40°. The substrate is kept at RT during deposition, except the dashed curve which is for a substrate at 400 K.

of Au at the $Au_{100-x}Cr_x$ alloy surface is not surprising.

According to Ref. 25, at $T=0$ K, the surface energy of Cr is 2400 mJ/m^2 as compared to 1550 mJ/m^2 for Au surfaces. The formation of a surface alloy with an Au-rich surface is just one way to reduce the very large surface energy of a uniform ultrathin Cr film on Au(100).

IV. FORMATION OF EPITAXIAL bcc Cr FILMS

A. Photoemission evidence

Quite convincing evidence for epitaxial growth of bcc Cr on Au(100) comes from Fig. 7. This is a series of photoemission spectra for various Cr deposits on Au(100) held at RT. The photon energy is 21.2 eV and the emission plane is (001) with a polar angle of emission of 40° with respect to the surface normal. Also shown is the relevant spectrum from clean Cr (100) single-crystal surface. This collection geometry has been chosen for the 0.2- and 0.9-eV features, very characteristic of clean Cr(100). Previous studies have shown that the 0.9-eV feature reflects mainly surface-state emission[30,39] with a smaller component due to bulk emission.[30]

Let us now consider the evolution of the spectrum from Cr/Au(100) as a function of coverage. As already pointed out in Sec. III A, by ~4 ML the Cr 3*d* feature exhibits a splitting with peaks near 0.6 and 1.3 eV suggesting enhanced interaction between Cr species, i.e., the formation of a Cr-rich phase. Upon further deposition this structure persists up to ~6 ML and then evolves gradually towards the bcc Cr(100) signature. For $\Theta \geq 12$ ML, the spectra closely resemble the reference spectrum from clean Cr(100). Obviously the data of Fig. 7 indicate that an epitaxial Cr(100) film grows on top of the interfacial alloy on Au(100). The major difference between the Cr/Au(100) and Cr(100) spectra is in the features at 4.8 and 6.3 eV which are not present on clean Cr(100). This additional structure reflects emission from Au 5*d* states and a possible origin is emission from Au(100) or $Au_{100-x}Cr_x(100)$ substrate. However, as shown below, there is evidence for a film structure which is quite uniform in thickness rather than three-dimensional crystallites with bare substrate patches in between. Thus, for $\Theta \geq 10$ ML where the thickness of the film is large as compared to the electron escape depth, a different origin must be invoked. Actually the narrow shape of both features points towards an interpretation in terms of essentially isolated Au species. Since the solubility of Au in bcc Cr is very small, we attribute this structure to the 5*d* spin-orbit-split doublet from Au species segregated at the surface of the Cr film. The measured spin-orbit splitting of 1.5 eV is in excellent agreement with photoemission data from Au species dissolved in Si, for instance.[40] On increasing the substrate temperature one expects enhanced Au diffusion towards the film surface and in turn enhanced Au segregation. The dashed line in Fig. 7 relevant to 15 ML deposited on a substrate held at 400 K shows that this is indeed the case. Au segregation at the film surface is also reflected in the work-function data of Fig. 6. Since Au segregation is expected to increase the work function, this readily explains the significantly higher values observed for the 400-K substrate relative to the RT substrate. It is also interesting to note that the work function decreases steadily in the 10–60-ML range but remains always higher than measured on clean Cr(100): 3.90±0.1 eV (Ref. 41). Again, this behavior reflects the progressively smaller amount of Au capable to diffuse to the surface with increasing film thickness. Note that even by 60 ML deposited on the substrate at RT there is a very small amount of Au segregated at the film surface, accounting for the ~0.15-eV-higher work function relative to clean Cr(100).

B. LEED observations

The LEED observations for the substrate held at RT reveal that by 3 ML an important diffuse background becomes apparent but the pattern still remains (1×1). By 5 ML the (1×1) spots are very faint with a dominant nonuniform diffuse background. Surprisingly, on further Cr deposition the (1×1) pattern reappears progressively and for coverages above 6 ML a low background (1×1) diagram can be observed again. This diagram is found to persist with little change up to 60 ML, the largest coverage investigated in this study. This implies that in the intermediate 4–6-ML range the phase formed on top of the epitaxial $Au_{100-x}Cr_x$ alloy is disordered. In fact, once the Cr concentration in the top layer exceeds the limiting solubility of Cr in Au (i.e., by ~3 ML at RT), only a disordered Au-Cr phase can be formed since according to the phase diagram there are no ordered $Au_{100-x}Cr_x$ alloys for $x \geq 50$. Apparently at this stage the Au concentration in the top layer remains sufficient to prevent nucleation of bcc Cr which according to the phase diagram is not able to dissolve a substantial amount of Au, exceeding 0.05 at. % or so.[24] On further Cr deposition the Cr concentration increases progressively since the Au supply is limited by diffusion and eventually the end phase, i.e., bcc Cr (with a very small amount of Au in solution) begins to nucleate. LEED suggests that this happens near 6 ML and the bcc Cr film grown in this way must be epitaxial. In the intermediate 4–6-ML coverage range, one observes indeed a qualitative modification in the LEED *I-V* curves which change from a shape characteristic of the ordered $Au_{100-x}Cr_x$ epitaxial alloy ($x \leq 50$) to a shape similar to that of a single-crystal Cr(100) surface. Finally, it is noteworthy that the diffraction spot width shows a pulsating behavior versus primary beam energy. This reveals the presence of steps with a random distribution of terrace widths[42] and in turn significant deviations from simple layer-by-layer growth. In this respect let us consider the Au $4f_{7/2}$ core line intensities versus coverage shown in Fig. 8. The data show a good fit to an exponential attenuation rate for a mean free path of ~15 ML or 21 Å in the case of a substrate held at RT. At higher temperatures, the important Au segregation obscures the interpretation. The RT result suggests a quite uniform Cr film thickness in spite of the high surface energy of Cr which in principle favors the formation of three-dimensional crystallites. Note, however, that Au segregation probably reduces the surface energy and stabilizes the thin-film structure. Thus we believe that the

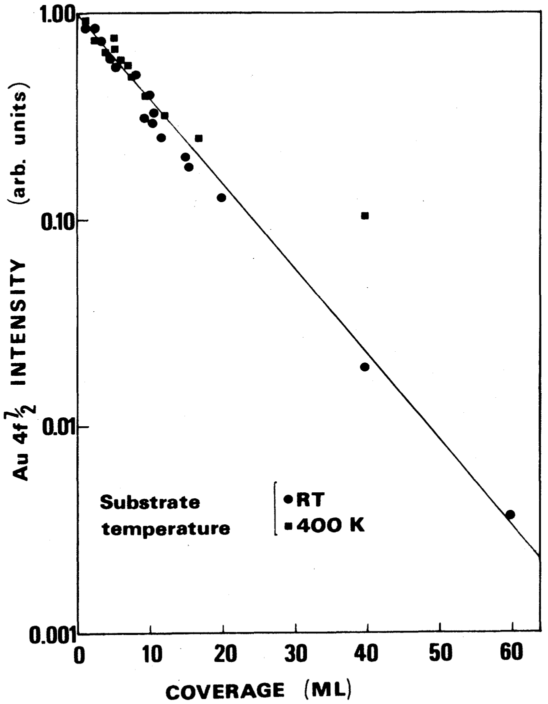

FIG. 8. Au $4f_{7/2}$ core line intensity change as a function of Cr coverage for the Cr/Au(100) interface formed either at RT or 400 K. The exponential attenuation rate yields a mean escape depth of ~21 Å for the Au $4f_{7/2}$ electrons in Cr.

film surface exhibits a stepped structure at the scale of the monolayer height but the overall film thickness seems to be fairly uniform. More detailed structural information can hardly be extracted from the results of Fig. 8 because of the large scattering in the data points. This is due to the fact that each measurement belongs to a separate experiment. Actually, after the measurements relevant to a given Cr deposit, the substrate has to be recleaned because of the very high reactivity of Cr.

C. Valence-band structure of the epitaxial Cr films

Figures 9 and 10 present angle-resolved photoemission spectra versus polar angle of emission taken with $\hbar\omega=21.2$ eV on clean Cr(100) for the (001) and $(0\bar{1}1)$ emission planes, respectively. The relevant data collected in exactly the same conditions for a 15-ML RT-formed Cr film on Au(100) are displayed in Figs. 11 and 12, respectively. A glance at these spectra reveals the striking one-to-one correspondence between both series of spectra. This leaves no doubt about the epitaxial bcc structure of the Cr films grown on Au(100) above 10 ML. The actual spectral differences still observed between clean Cr(100) and epitaxial Cr films on Au(100) can be traced back to differences in the surface electronic structure. As pointed out above, Au segregation at the film surface is responsible for the 4.8 and 6.3 eV peaks in the epitaxial film spectra. A remarkable consequence of this segregation is a significant reduction in the intensity of the surface state observed at normal emission at 0.65 eV on clean Cr(100). Previous work[13,39,43] has shown that this

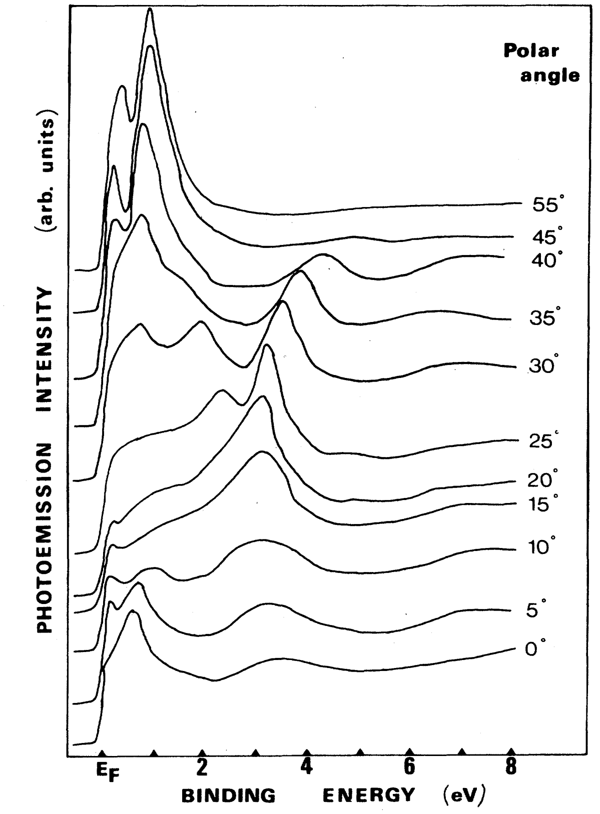

FIG. 9. Off-normal emission spectra, taken with $\hbar\omega=21.2$ eV for clean Cr(100), as a function of polar angle of emission in the (001) plane. The light incidence angle is 45°.

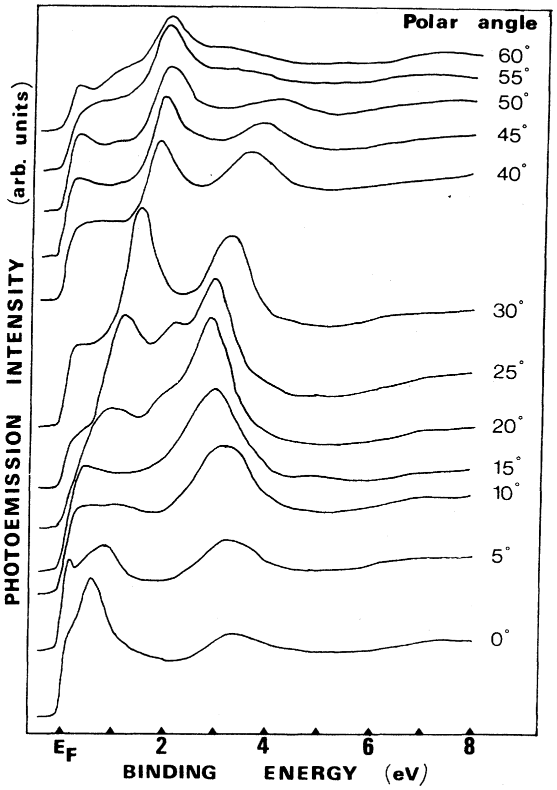

FIG. 10. Same as Fig. 9 but for the $(0\bar{1}1)$ emission plane.

feature is extremely sensitive to surface contamination or surface disorder. Possibly the disorder inherent in the stepped film surface also contributes to the attenuation of this feature. Another small structure is visible at normal emission near 0.1 eV in the epitaxial film spectrum but not in our single-crystal spectrum. However, since Klebanoff *et al.* in their Cr(100) spectra also observe a similar feature[39] we conclude that this is characteristic of Cr(100) though in our Cr(100) spectra such a feature becomes visible only at collection angles slightly off-normal.

The majority of the prominent peaks in the spectra reflect direct transitions from bulk states. A notable exception, already mentioned in Sec. IV A, is the conspicuous feature near 1 eV at large polar angles α. Considering now the bulk transitions it was demonstrated in Ref. 13 that off-normal emission spectra in the $(0\bar{1}1)$ plane probe Brillouin zone points very close to the HN symmetry line for $\hbar\omega = 16.8$ eV and $0° < \alpha < 45°$ or $\hbar\omega = 21.2$ eV and $25° < \alpha < 50°$. A similar statement holds for the ΓH symmetry line and emission in the (001) plane. Thus, using the data taken with Ne I and He I radiation from a 40-ML Cr film we can determine the relevant band dispersions as for Cr(100) in Ref. 13. The direct transition model assumes a free-electron final-state band dispersion with an inner potential $V_0 = 10.8$ eV. The data are shown as circles in Fig. 13 where the continuous lines represent the experimental band structure deduced previously from Cr(100) single-crystal measurements.[13] The amount of available data is limited but where a comparison can be made the agreement is excellent.

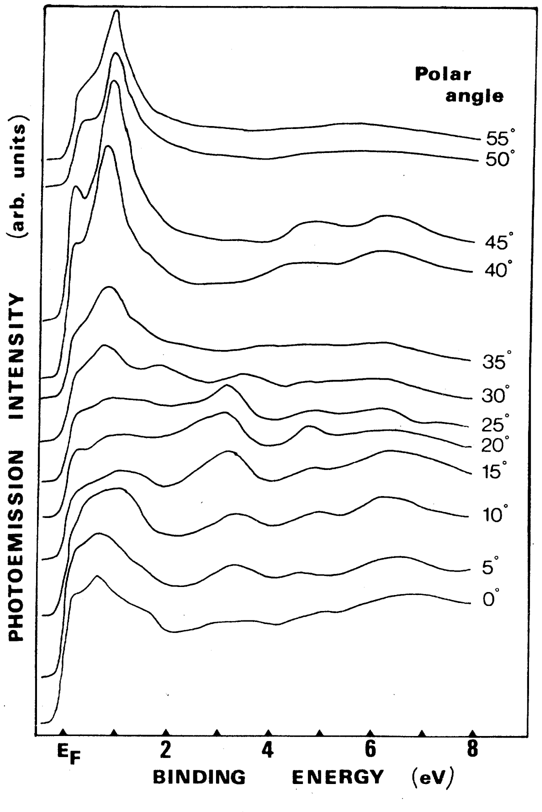

FIG. 11. Off-normal emission spectra, taken with $\hbar\omega = 21.2$ eV for 15 ML of Cr deposited on Au(100) held at RT, as a function of polar angle of emission in the (001) plane. The light incidence angle is 45°.

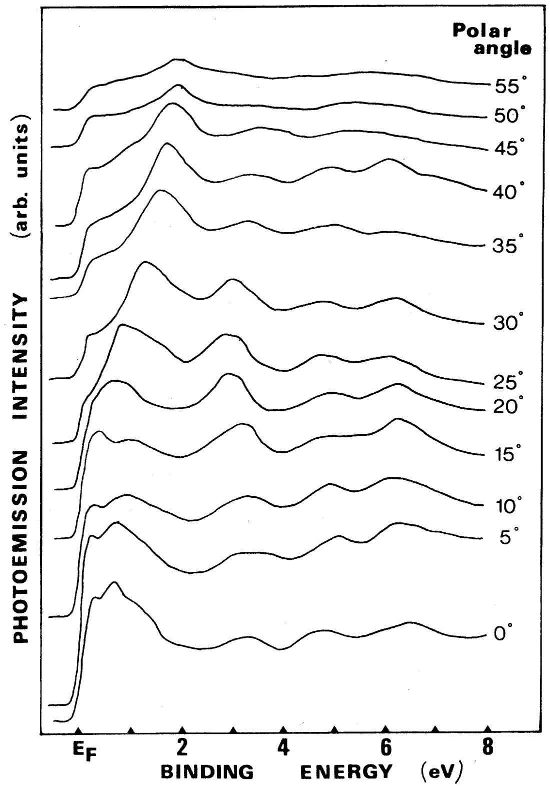

FIG. 12. Same as Fig. 11 but for the $(0\bar{1}1)$ emission plane.

Finally, let us consider the case of very thin Cr films in

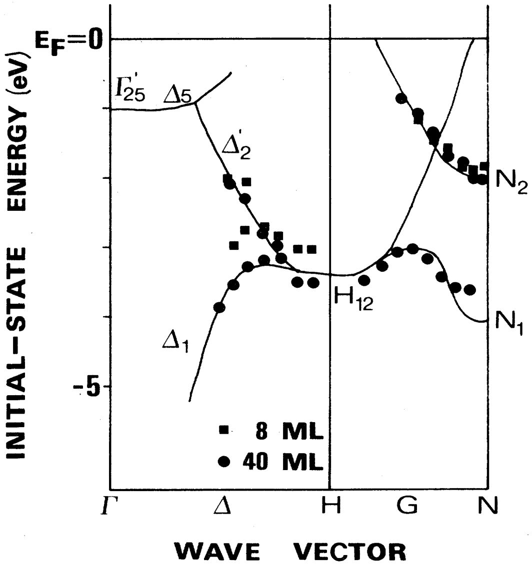

FIG. 13. Experimental band structures for 8 and 40 ML of Cr deposited on Au(100) held at RT. The continuous lines represent the experimental band structure for bulk Cr reported in Ref. 13. The data are presented in the paramagnetic Brillouin zone as in Ref. 13 for comparison.

the 6–10-ML range. Figure 7 indicates the progressive appearance of the typical transitions of bcc Cr in that coverage range. Keeping in mind the presence of the interfacial alloy, the effective Cr film thickness in that range is expected to vary from ∼3 to 7 ML. Two observations are noteworthy. First, on reducing the film thickness, the intensity of spectral features progressively decreases and their energy location shifts away from the limiting bulk position. This shift is quite visible in Fig. 7 for the prominent feature near 0.9 eV which moves towards lower binding energies in ultrathin Cr layers. Second, the intensity of some transitions is particularly sensitive to the film thickness reduction. This is the case for the 0.2-eV peak in the spectra of Fig. 7.

To see more specifically these effects we have also represented as squares in Fig. 13 the experimental band structure along ΓH for an 8-ML film deposited at RT using the same method as for the 40-ML film. An estimation of the effective film thickness taking into account the presence of the interfacial alloy is ∼4 ML. One observes a substantial shift (∼0.4 eV) to lower binding energy of the Δ_1 band near H_{12} and a disappearance of the transitions from the rapidly dispersing Δ_2' band. In contrast, note that little change is visible near N_2. Since H_{12} is a $3d$ band edge these observations suggest a d band narrowing associated with the reduced film size. In very thin films it is also expected that $k_\perp$ is no longer a good quantum number and the direct-transition model of photoemission breaks down. Direct photoemission transitions from rapidly dispersing bands are then more strongly affected than emission from flat bands.

Alternatively, these effects might result from the presence of Au in these ultrathin films. We have shown that Au is capable to diffuse to the film surface. Yet the solubility of Au in bcc Cr seems too small to account for the strong perturbation in the band structure observed near H_{12}.

The possibility of enhanced magnetism might also be responsible for the changes in the band structure of ultrathin films. Our core-level data such as the Cr $2s$ multiplet splitting do not indicate the presence of a local magnetic moment much stronger than in bulk Cr for the Cr overlayers on top of the interfacial alloy. However, the low resolution and signal-to-noise ratio precludes a precise evaluation of the local moment from our data. Note also that a critical discussion of XPS data shows a poor correlation between the Fe $3s$ splitting and the magnetic moment in alloys and inorganic compounds.[44] Nevertheless, in a recent study of the Cr/Ag (100) system, Newstead *et al.*[17] also arrive at the conclusion that the moment in ultrathin Cr layers is considerably less than predicted theoretically.[8,9]

V. CONCLUSION

We have shown that the first monolayers of Cr on Au form an epitaxial substitutional alloy which acts as a good template for epitaxial growth of bcc Cr films. These Cr films have a fairly uniform thickness but exhibit a stepped surface. Distinct deviations from bulk electronic structure are visible in ultrathin films. However, the presence of the interfacial alloy complicates the interpretation of these thin-film effects. In addition, since this alloy is itself magnetic, its presence also obscures the investigation of the possibly enhanced magnetism in ultrathin Cr films. The Cr/Ag(100) system seems to be a better choice for such studies since Ag is immiscible with Cr and the mismatch in the lattice parameters is also very small. Note however, that interdiffusion of overlayer and substrate is one way to relief of misfit strain at the interface. Furthermore, Au segregation at the Cr surface also reduces the very large excess of surface energy of ultrathin Cr films on Au(100) relative to clean Au(100). Clearly, this stabilizes the thin-film structure on Au(100). The absence of this stabilizing effect at the Cr/Ag(100) interface might well favor the growth of three-dimensional crystallites rather than a uniform ultrathin film.

Finally, in a recent paper[45] O'Neill and Weaver also present photoemission measurements on the Cr/Au(100) interface but interpret their data in a layer-by-layer growth model. In our opinion, these authors do not present convincing evidence for but rather assume implicitly that growth mode in their comparison of the Cr-derived electronic structure with theoretical calculations based on an atomically sharp interface model. We believe that the data of Ref. 45 should be reinterpreted in the light of the above findings.

---

[1] See, for instance, E. Bauer and J. H. van der Merwe, Phys. Rev. B **33**, 3657 (1986); J. G. Tobin, S. W. Robey, and D. A. Shirley, *ibid.* **33**, 2270 (1986), and references therein.

[2] J. G. Tobin, S. W. Robey, L. E. Klebanoff, and D. A. Shirley, Phys. Rev. B **35**, 9056 (1987).

[3] A. L. Wachs, A. P. Shapiro, T. C. Hsieh, and T. C. Chiang, Phys. Rev. B **33**, 1460 (1986).

[4] G. Zajac, S. D. Bader, and R. J. Friddle, Phys. Rev. B **31**, 4947 (1985).

[5] M. B. Brodsky, P. Marikar, R. J. Friddle, L. Singer, and G. H. Sowers, Solid State Commun. **42**, 675 (1982).

[6] M. B. Brodsky, J. Appl. Phys. **52**, 1665 (1981).

[7] M. B. Brodsky, J. Magn. Magn. Mater. **35**, 99 (1983).

[8] C. L. Fu, A. J. Freeman, and T. Oguchi, Phys. Rev. Lett. **54**, 2700 (1985).

[9] C. L. Fu and A. J. Freeman, Phys. Rev. B **33**, 1611 (1986).

[10] M. C. Hanf, C. Pirri, J. C. Peruchetti, D. Bolmont, and G. Gewinner, Phys. Rev. B **36**, 4487 (1987).

[11] J. S. Foord and R. M. Lambert, Surf. Sci. **115**, 141 (1982).

[12] G. Gewinner, J. C. Peruchetti, and A. Jaegle, Surf. Sci. **122**, 383 (1982).

[13] G. Gewinner, J. C. Peruchetti, and A. Jaegle, Phys. Rev. B **27**, 3358 (1983).

[14] M. C. Hanf, C. Pirri, J. C. Peruchetti, D. Bolmont, and G. Gewinner, Phys. Rev. B (to be published).

[15] P. Heimann, J. Hermanson, H. Miosga, and H. Neddermeyer Phys. Rev. Lett. **43**, 1757 (1979).

[16] H. S. Reehal and P. T. Andrews, J. Phys. F **10**, 1631 (1980).

[17] D. A. Newstead, C. Norris, C. Binns, and P. C. Stephenson, J. Phys. C **20**, 6245 (1987).

[18] M. C. Hanf, L. Haberbache, P. Wetzel, C. Pirri, J. C. Peruchetti, D. Bolmont, and G. Gewinner, Solid State Commun. **68**, 113 (1988).

[19] N. J. Shevchik, J. Phys. F **5**, 1860 (1975).

[20] J. A. Nicholson, J. D. Riley, R. C. G. Leckey, J. G. Jenkin, J. Liesegang, and J. Azoulay, Phys. Rev. B **18**, 2561 (1978).

[21] J. S. Friedel, Nuovo Cimento Suppl. **111**, 287 (1958).

[22] J. L. Beeby, Phys. Rev. **135**, A130 (1964).

[23] B. Velicky, S. Kirkpatrick, and H. Ehrenreich, Phys. Rev. **175**, 747 (1968).

[24] E. Raub, Z. Metallkd. **51**, 290 (1960).

[25] A. R. Miedema, P. F. de Châtel, and F. R. de Boer, Physica B+C **100B**, 1 (1980).

[26] E. Wachtel and U. Vetter, Z. Metallkd. **52**, 525 (1980).

[27] Y. Nakai, M. Sakuma, and N. Kunitomi, J. Phys. Soc. Jpn. **56**, 301 (1987).

[28] J. H. Van Vleck, Phys. Rev. **45**, 405 (1934).

[29] D. A. Shirley, in *Photoemission in Solids,* edited by M. Cardona and L. Ley (Springer, Berlin, 1978), Vol. 1.

[30] G. Gewinner, Thèse d'Etat, Université de Haute Alsace, France, 1983 (unpublished).

[31] S. P. Kowalczyk, L. Ley, F. R. McFeely, and D. A. Shirley, Phys. Rev. B **11**, 1721 (1975).

[32] R. P. Gupta and S. K. Sen, Phys. Rev. B **10**, 71 (1974).

[33] B. H. Verbeek, Solid State Commun. **44**, 951 (1982).

[34] P. Steiner, S. Hüfner, N. Martensson, and B. Johansson, Solid State Commun. **37**, 73 (1981).

[35] G. Tréglia, M. C. Desjonquères, D. Spanjaard, Y. Lassailly, C. Guillot, Y. Jugnet, Tran Minh Duc, and J. Lecante, J. Phys. C **14**, 3463 (1981).

[36] G. Apai, R. C. Baetzold, P. J. Jupiter, A. J. Viescas, and I. Lindau, Surf. Sci. **134**, 122 (1983).

[37] R. E. Watson, J. Hudis, and M. L. Perlman, Phys. Rev. B **4**, 4139 (1971).

[38] D. G. O'Neill and J. H. Weaver, Phys. Rev. B **35**, 5892 (1987).

[39] L. E. Klebanoff, R. H. Victora, L. M. Falicov, and D. A. Shirley, Phys. Rev. B **32**, 1997 (1985).

[40] M. Iwami, T. Terada, H. Tochihara, M. Kubota, and Y. Murata, Surf. Sci. **194**, 115 (1988).

[41] J. C. Peruchetti, C. Pirri, D. Bolmont, and G. Gewinner, Solid State Commun. **59**, 517 (1986).

[42] M. Henzler, in *Electron Spectroscopy for Surface Analysis,* edited by H. Ibach (Springer, Berlin, 1977), Vol. 4.

[43] L. E. Klebanoff, S. W. Robey, G. Liu, and D. A. Shirley, Phys. Rev. B **31**, 6379 (1985).

[44] J. F. van Acker, Z. M. Stadnik, J. C. Fuggle, H. J. W. M. Hoekstra, K. H. J. Buschow, and G. Stoink, Phys. Rev. B **37**, 6827 (1988).

[45] D. G. O'Neill and J. H. Weaver, Phys. Rev. B **37**, 8122 (1988).